Three-dimensional efficient dispersive alternating-direction-implicit finite-difference time-domain algorithm using a quadratic complex rational function

E.-K. Kim,[1] S.-G. Ha,[1] J. Lee,[2] Y. B. Park,[3] and K.-Y. Jung[1,*]

[1] *Department of Electronics and Computer Engineering, Hanyang University, 222,*
Wangsimni-ro, Seongdong-gu, Seoul 133-971, South Korea
[2] *The 7th R&D Institute-3, Agency for Defense Development*
330 Shin-seong Road, Haemi-myeon, Seosan-si, Chungcheongnam-do 356-823, South Korea
[3] *Department of Electrical and Computer Engineering, Ajou University, 206, World cup-ro*
Suwon 443-749, South Korea

[*] *kyjung3@hanyang.ac.kr*

Abstract: Efficient unconditionally stable FDTD method is developed for the electromagnetic analysis of dispersive media. Toward this purpose, a quadratic complex rational function (QCRF) dispersion model is applied to the alternating-direction-implicit finite-difference time-domain (ADI-FDTD) method. The 3-D update equations of QCRF-ADI-FDTD are derived using Maxwell's curl equations and the constitutive relation. The periodic boundary condition of QCRF-ADI-FDTD is discussed in detail. A 3-D numerical example shows that the time-step size can be increased by the proposed QCRF-ADI-FDTD beyond the Courant-Friedrich-Levy (CFL) number, without numerical instability. It is observed that, for refined computational cells, the computational time of QCRF-ADI-FDTD is reduced to 28.08 % of QCRF-FDTD, while the L_2 relative error norm of a field distribution is 6.92 %.

References and links

1. A. Taflove and S. C. Hagness, *Computational Electrodynamics: The Finite-Difference Time-Domain Method* (Artech House, 3rd ed., 2005).
2. I.-Y. Oh, Y. Hong, and J.-G. Yook, "Extremely low numerical dispersion FDTD method based on H(2,4) scheme of lossy material," J. Electromagn. Eng. Sci. **13**(3), 158–164 (2013).
3. K.-Y. Jung, F. L. Teixeira, and R. M. Reano, "Surface plasmon coplanar waveguides: Mode characteristics and mode conversion losses," IEEE Photon. Technol. Lett. **21**(10), 630–632 (2009).
4. K.-Y. Jung, S. Ju, and F. L. Teixeira, "Application of the modal CFS-PML-FDTD to the analysis of magnetic photonic crystal waveguides," IEEE Microw. Wireless Compat. Lett. **21**(4), 179–181 (2011).
5. S. K. Pradhan, B. Xiao, J. R. Skuza, K. Santiago, R. Mundle, and A. K. Pradhan, "Effects of dielectric thickness on optical behavior and tunability of one-dimensional Ag/SiO$_2$ multilayered metamaterials," Opt. Express **22**(10), 12486–12498 (2014).

6. J. W. Lim, Y. T. Lee, R. Pandey, T.-H. Yoo, B.-I. Sang, B.-K. Ju, D. K. Hwang, and W. K. Choi, "Effect of geometric lattice design on optical/electrical properties of transparent silver grid for organic solar cells," Opt. Express **22**(22), 26891–26899 (2014).
7. S.-G. Ha, J. Cho, J. Choi, H. Kim, and K.-Y. Jung, "FDTD dispersive modeling of human tissue based on quadratic complex rational function," IEEE Trans. Antennas Propagat. **61**(2), 996–999 (2013).
8. H. Chung, J. Cho, S.-G. Ha, S. Ju, and K.-Y. Jung, "Accurate FDTD dispersive modeling for concrete materials," ETRI J. **35**(5), 915–918 (2013).
9. H. Chung, K.-Y. Jung, X. T. Tee, and P. Bermel, "Time domain simulation of tandem silicon solar cells with optimal textured light trapping enabled by the quadratic complex rational function," Opt. Express **22**(S3), A818–A832 (2014).
10. T. Wuren, T. Takai, M. Fujii, and I. Sakagami, "Effective 2-Debye-pole FDTD model of electromagnetic interaction between human body and UWB radiation," IEEE Microw. Wireless Compat. Lett. **17**(7), 483–485 (2007).
11. K.-Y. Jung, F. L. Teixeira, and R. M. Reano, "Au/SiO$_2$ nanoring plasmon waveguides at optical communication band," J. Lightw. Technol. **25**(9), 2757–2765 (2007).
12. S. Aksoy, "An alternative algorithm for both narrowband and wideband Lorentzian dispersive materials modeling in the finite-difference time-domain method," IEEE Trans. Microw. Theory Tech. **55**(4), 703-708 (2007).
13. W.-J. Yoon, K.-Y. Jung, J. Liu, T. Duraisamy, R. Revur, F. L. Teixeira, S. Sengupta, and P. R. Berger, "Plasmon-enhanced optical absorption and photocurrent in organic bulk heterojunction photovoltaic devices using self-assembled layer of silver nanoparticles," Sol. Energy Mater. Sol. Cells **94**(2), 128–132 (2010).
14. D. Y. Na, J. H. Kim, K.-Y. Jung, and Y. B. Park, "Mode-matching analysis of a coaxially fed annular slot surrounded with corrugations," Electromagn. **34**(2), 92–110 (2014).
15. S. Buil, J. Laverdant, B. Berini, P. Maso, J.-P. Hermier, and X. Quélin, "FDTD simulations of localization and enhancements on fractal plasmonics nanostructures," Opt. Express **20**(11), 11968–11975 (2012).
16. F. Zheng, "A finite-difference time-domain method without the courant stability conditions," IEEE Microwave Guided Wave Let. **9**(11), 441–443 (1999).
17. K.-Y. Jung and F. L. Teixeira, "Multispecies ADI-FDTD algorithm for nanoscale three-dimensional photonic metallic structures," IEEE Photon. Technol. Lett. **19**(8), 586–588 (2007).
18. K.-Y. Jung, F. L. Teixeira, S. G. Garcia, and R. Lee, "On numerical artifacts of the complex envelope ADI-FDTD method," IEEE Trans. Antennas Propagat. **57**(2), 491–498 (2009).
19. J. W. Thomas, *Numerical Partial Differential Equations: Finite Difference Method* (Springer, 1995).
20. S. Gedney, G. Liu, J. Roden, and A. Zhu, "Perfectly matched layer media with CFS for an unconditionally stable ADI-FDTD method," IEEE Trans. Antennas Propagat. **49**(11), 1554–1559 (2001).
21. K.-Y. Jung, S. Ju, and F. L. Teixeira, "Two-stage perfectly matched layer for the analysis of plasmonic structures," IEICE Trans. Electronics, **E93-C**(8), 1371–1374 (2010)
22. S. Wang, J. Chen, and P. Ruchhoeft, "An ADI-FDTD method for periodic structures," IEEE Trans. Antennas Propagat. **53**(7), 2343–2346 (2005).
23. W. H. Press, S. A. Teukolsky, W. T. Vetterling, and B. P. Flannery, *Numerical Recipes: The Art of Scientific Computing* (Cambrige University, 3rd ed., 1995).
24. K.-Y. Jung and F. L. Teixeira, "An iterative unconditionally stable stable LOD-FDTD method," IEEE Microw. Wireless Compat. Lett. **18**(2), 76–78 (2008).
25. Q. H. Liu, "The PSTD algorithm: A time-domain method requiring only two cells per wavelength," Microwave Opt. Technol. Lett. **15**(3), 158–165 (1997).
26. M. W. Feise, J. B. Schneider, and P. J. Bevelacqua, "Finite-difference and pseudospectral time-domain methods applied to backward-wave metamaterials," IEEE Trans. Antennas Propagat. **52**(11), 2955–2962 (2004).
27. C. Liu, R. L. Panetta, and P. Yang, "Application of the pseudo-spectral time domain method to compute particle single-scattering properties for size parameters up to 200," J. Quant. Spectrosc. Radiat. Trans. **113**(13), 1728–1740 (2012).

1. Introduction

The finite-difference time-domain (FDTD) method [1] has been popularly applied for a wide range of electromagnetic (EM) problems including lossy materials [2], plasmonic structures [3], magnetic photonic crystals [4], metamaterials [5], and organic solar cells [6]. FDTD is accurate and robust, and also it can obtain wideband EM responses by performing a single simulation. In FDTD, due to the time-domain approach, a proper dispersion model is required for analyzing materials with frequency-dependent characteristics. Recently, the quadratic complex rational function (QCRF) dispersion model was successfully employed for the FDTD analysis of dispersive media, such as human tissues [7], concrete materials [8], and silicon solar cells [9]. The QCRF dispersion model has higher degree of freedom than Debye [10], Drude [11], or

Lorentz [12] models and also its coefficients can be obtained by a simple matrix calculation.

Due to the explicit solution of differential equations, the time-step size of FDTD is limited by the Courant-Friedrichs-Levy (CFL) stability limit [1] which is a function of minimum spatial grid sizes determined by the highest frequency and/or a given structure. When objects are much smaller than the wavelength of interests (e.g., thin film devices [13], subwavelength structures [14], or nanostructures [15]), a FDTD analysis is highly demanding. To overcome the CFL stability limit of FDTD, the alternating direction implicit (ADI)-FDTD can be used [16–18]. Since it involves an semi-implicit scheme, time-marching update equations can be calculated unconditionally stably by using a large time-step size beyond the CFL stability limit.

In this work, we apply the QCRF dispersion model to the ADI-FDTD algorithm to efficiently analyze optical wave propagation in dispersive media. The periodic boundary condition (PBC) is employed for the lateral computational cells to excite the plane wave with enhanced computational efficiency and the complex frequency-shifted (CFS) perfectly matched layer (PML) is used for the longitudinal direction to minimize spurious reflections from the computational boundary. Finally, a 3-D numerical example is used to illustrate the computational accuracy and efficiency of the proposed QCRF-ADI-FDTD.

2. Methodology

Before proceeding with the formulation of QCRF-ADI-FDTD, we briefly review the formulation of QCRF-FDTD [7]. We assume the $e^{j\omega t}$ time convention in what follows, where $j = \sqrt{-1}$.

2.1. Formulation of QCRF-FDTD

In QCRF-FDTD, the relative permittivity part of a dispersive medium is expressed as

$$\varepsilon_r(\omega) = \frac{A_0 + A_1(j\omega) + A_2(j\omega)^2}{1 + B_1(j\omega) + B_2(j\omega)^2} \tag{1}$$

where A_0, A_1, A_2, B_1, B_2 are the real coefficients which can be simply obtained by a 5×5 matrix calculation [7]. In order to obtain the update equations of QCRF-FDTD, we consider the constitutive relation as follows

$$\mathbf{D}(\omega) = \varepsilon_0 \left(\frac{A_0 + A_1(j\omega) + A_2(j\omega)^2}{1 + B_1(j\omega) + B_2(j\omega)^2} \right) \mathbf{E}(\omega). \tag{2}$$

By applying the inverse Fourier transform and the central difference scheme (CDS), we have

$$\frac{\mathbf{D}^{n+1} + 2\mathbf{D}^n + \mathbf{D}^{n-1}}{4} + B_1 \frac{\mathbf{D}^{n+1} - \mathbf{D}^{n-1}}{2\Delta t} + B_2 \frac{\mathbf{D}^{n+1} - 2\mathbf{D}^n + \mathbf{D}^{n-1}}{\Delta t^2} \tag{3}$$
$$= \varepsilon_0 A_0 \frac{\mathbf{E}^{n+1} + 2\mathbf{E}^n + \mathbf{E}^{n-1}}{4} + \varepsilon_0 A_1 \frac{\mathbf{E}^{n+1} - \mathbf{E}^{n-1}}{2\Delta t} + \varepsilon_0 A_2 \frac{\mathbf{E}^{n+1} - 2\mathbf{E}^n + \mathbf{E}^{n-1}}{\Delta t^2}.$$

With some manipulations, final update equation for $\mathbf{E}$ can be obtained as follows

$$\mathbf{E}^{n+1} = C_a \mathbf{E}^n + C_b \mathbf{E}^{n-1} + C_c \mathbf{D}^{n+1} + C_d \mathbf{D}^n + C_e \mathbf{D}^{n-1} \tag{4}$$

where $C_a = -2(\alpha_0 - \alpha_2)/(\alpha_0 + \alpha_1 + \alpha_2)$, $C_b = -(\alpha_0 - \alpha_1 + \alpha_2)/(\alpha_0 + \alpha_1 + \alpha_2)$, $C_c = (\beta_0 + \beta_1 + \beta_2)/(\alpha_0 + \alpha_1 + \alpha_2)$, $C_d = 2(\beta_0 - \beta_2)/(\alpha_0 + \alpha_1 + \alpha_2)$, and $C_e = (\beta_0 - \beta_1 + \beta_2)/(\alpha_0 + \alpha_1 + \alpha_2)$. Note that $\alpha_0 = A_0(\Delta t)^2$, $\alpha_1 = 2A_1\Delta t$, $\alpha_2 = 4A_2$, $\beta_0 = (\Delta t)^2/\varepsilon_0$, $\beta_1 = 2B_1\Delta t/\varepsilon_0$, and $\beta_2 = 4B_2/\varepsilon_0$. In above, the superscript refers to the time-step indexing. The update equations of $\mathbf{D}$ and $\mathbf{H}$ can be obtained by applying the CDS to time-dependent Maxwell's curl equations.

2.2. Formulation of QCRF-ADI-FDTD

The ADI scheme requires updating EM field components from the time step n to $n+1$ through two sub-iterations. Therefore, QCRF-ADI-FDTD update equations of $\mathbf{E}$ can be written as

First sub-iteration:

$$\mathbf{E}^{n+1/2} = C_c\mathbf{D}^{n+1/2} + \boldsymbol{\phi}^n \tag{5}$$

$$\boldsymbol{\phi}^{n+1/2} = C_a\mathbf{E}^{n+1/2} + C_b\mathbf{E}^n + C_d\mathbf{D}^{n+1/2} + C_e\mathbf{D}^n \tag{6}$$

Second sub-iteration:

$$\mathbf{E}^{n+1} = C_c\mathbf{D}^{n+1} + \boldsymbol{\phi}^{n+1/2} \tag{7}$$

$$\boldsymbol{\phi}^{n+1} = C_a\mathbf{E}^{n+1} + C_b\mathbf{E}^{n+1/2} + C_d\mathbf{D}^{n+1} + C_e\mathbf{D}^{n+1/2}. \tag{8}$$

Note that C_a, C_b, C_c, C_d, and C_e are same as in FDTD but with different variables: $\alpha_0 = A_0(\Delta t)^2/4$, $\alpha_1 = A_1\Delta t$, $\alpha_2 = 4A_2$, $\beta_0 = (\Delta t)^2/(4\varepsilon_0)$, $\beta_1 = B_1\Delta t/\varepsilon_0$, and $\beta_2 = 4B_2/\varepsilon_0$. Similar to $\mathbf{E}$ update equations, the update equations of $\mathbf{D}$ and $\mathbf{H}$ at each time step is divided into two sub-iterations and they can be obtained from time-dependent Maxwell's curl equations. For example, the first sub-step update equations of the $D_x^{n+1/2}$ and $H_z^{n+1/2}$ are derived as

$$D_x|_{i+1/2,j,k}^{n+1/2} = D_x|_{i+1/2,j,k}^n + \frac{\Delta t}{2\Delta y}(H_z|_{i+1/2,j+1/2,k}^{n+1/2} - H_z|_{i+1/2,j-1/2,k}^{n+1/2}) \tag{9}$$
$$- \frac{\Delta t}{2\Delta z}(H_y|_{i+1/2,j,k+1/2}^n - H_y|_{i+1/2,j,k-1/2}^n)$$

$$H_z|_{i+1/2,j+1/2,k}^{n+1/2} = H_z|_{i+1/2,j+1/2,k}^n - \frac{\Delta t}{2\mu_0\Delta x}(E_y|_{i+1,j+1/2,k}^n - E_y|_{i,j+1/2,k}^n) \tag{10}$$
$$+ \frac{\Delta t}{2\mu_0\Delta y}(E_x|_{i+1/2,j+1,k}^{n+1/2} - E_x|_{i+1/2,j,k}^{n+1/2})$$

where the subscript refers to the spatial grid indexing. Note that we cannot solve $D_x^{n+1/2}$ and $H_z^{n+1/2}$ directly from Eqs. (9) and (10), because field values at the simultaneous time $(n+1/2)$ are involved. Therefore, plugging Eq. (5) into Eq. (10) and then putting the resulting equation into Eq. (9), we have

$$-\frac{C_0D_0C_c}{(\Delta y)^2}D_x|_{i+1/2,j-1,k}^{n+1/2} + \left[1 + 2\frac{C_0D_0C_c}{(\Delta y)^2}\right]D_x|_{i+1/2,j,k}^{n+1/2} - \frac{C_0D_0C_c}{(\Delta y)^2}D_x|_{i+1/2,j+1,k}^{n+1/2} \tag{11}$$
$$= D_x|_{i+1/2,j,k}^n + \frac{C_0}{\Delta y}\left(H_z|_{i+1/2,j+1/2,k}^n - H_z|_{i+1/2,j-1/2,k}^n\right)$$
$$- \frac{C_0}{\Delta z}\left(H_y|_{i+1/2,j,k+1/2}^n - H_y|_{i+1/2,j,k-1/2}^n\right)$$
$$- \frac{C_0D_0}{\Delta y\Delta x}\left(E_y|_{i+1,j+1/2,k}^n - E_y|_{i,j+1/2,k}^n - E_y|_{i+1,j-1/2,k}^n + E_y|_{i,j-1/2,k}^n\right)$$
$$+ \frac{C_0D_0}{(\Delta y)^2}\left(\phi_x|_{i+1/2,j-1,k}^n - 2\phi_x|_{i+1/2,j,k}^n + \phi_x|_{i+1/2,j+1,k}^n\right)$$

where $C_0 = \Delta t/2$ and $D_0 = \Delta t/(2\mu_0)$. Note that Eq. (11) can be efficiently solved by the Thomas algorithm [19]. Overall, the 3-D QCRF-ADI-FDTD procedure in the first sub-iteration is summarized as

1. Implicitly update $\mathbf{D}^{n+1/2}$ (e.g., Eq. (11))

2. Explicitly update $\mathbf{E}^{n+1/2}$ (e.g., Eq. (5))

3. Explicitly update $\boldsymbol{\phi}^{n+1/2}$ (e.g., Eq. (6))

4. Explicitly update $\mathbf{H}^{n+1/2}$ (e.g., Eq. (10)).

An analogous procedure can be applied for deriving the update equations of QCRF-ADI-FDTD in the second sub-iteration. In this work, the CFS-PML [20] is employed to minimize spurious reflection from the outer grid boundaries along the longitudinal (z) direction. By using a complex stretched coordinate technique [21], the CFS-PML implementation of QCRF-ADI-FDTD can be straightforwardly obtained and thus details are omitted in this paper. On the other hand, we employ the PBC [22] on the lateral (x and y) direction to efficiently excite the plane wave and details on the PBC implementation of QCRF-ADI-FDTD will be discussed in the next section.

2.3. Periodic boundary condition of QCRF-ADI-FDTD

When applying the PBC to QCRF-ADI-FDTD, the update equations of $\mathbf{D}$ do not have a tridiagonal matrix form anymore. Without loss of generality, we consider the y directional periodicity. We can write the update equation of D_x in the first sub-iteration as a cyclic tridiagonal matrix form $[\mathbf{M}]\mathbf{x} = \mathbf{r}$

$$[\mathbf{M}] = \begin{bmatrix} b_0 & c_0 & 0 & 0 & a_{N-1} \\ a_1 & b_1 & c_1 & 0 & 0 \\ 0 & \ddots & \ddots & \ddots & 0 \\ 0 & 0 & a_{N-2} & b_{N-2} & c_{N-2} \\ c_0 & 0 & 0 & a_{N-1} & b_{N-1} \end{bmatrix}, \ \mathbf{x} = \begin{bmatrix} D_x|_{i+1/2,0,k}^{n+1/2} \\ \vdots \\ D_x|_{i+1/2,j,k}^{n+1/2} \\ \vdots \\ D_x|_{i+1/2,N-1,k}^{n+1/2} \end{bmatrix}, \ \mathbf{r} = \begin{bmatrix} r|_0^n \\ \vdots \\ r|_j^n \\ \vdots \\ r|_{N-1}^n \end{bmatrix}. \quad (12)$$

Let us consider the PBC at j=0. As seen from Eq. (11) and Fig. 1(a), to update $D_x|_{i+1/2,0,k}^{n+1/2}$, we need $H_z|_{i+1/2,-1/2,k}^n$, $E_y|_{i+1,-1/2,k}^n$, $E_y|_{i,-1/2,k}^n$, and $\phi_x|_{i+1/2,-1,k}^n$. They are not allocated in the computer memory and thus we use alternative field values using the periodicity:

$$H_z|_{i+1/2,-1/2,k}^n \leftarrow H_z|_{i+1/2,N-1/2,k}^n \qquad (13)$$
$$E_y|_{i+1,-1/2,k}^n \leftarrow E_y|_{i+1,N-1/2,k}^n$$
$$E_y|_{i,-1/2,k}^n \leftarrow E_y|_{i,N-1/2,k}^n$$
$$\phi_x|_{i+1/2,-1,k}^n \leftarrow \phi_x|_{i+1/2,N-1,k}^n.$$

When updating $D_x|_{i+1/2,j,k}^{n+1/2}$ at j=N (see Fig. 1(b)), we can simply use the filed value at j=0:

$$D_x|_{i+1/2,N,k}^{n+1/2} \leftarrow D_x|_{i+1/2,0,k}^{n+1/2}. \qquad (14)$$

For updating $D_z|_{i,0,k+1/2}^{n+1/2}$, we need $H_x|_{i,-1/2,k+1/2}^n$ and we can use the following relation:

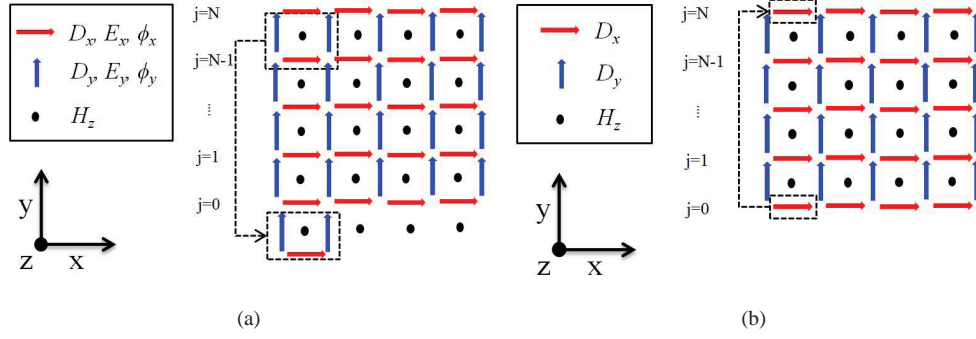$$H_x|_{i,-1/2,k+1/2}^n \leftarrow H_x|_{i,N-1/2,k+1/2}^n. \qquad (15)$$

Fig. 1. Field location in the computational cell. (a) updating $D_x^{n+1/2}$ at $j=0$. (b) updating $D_x^{n+1/2}$ at $j=N$.

Also, we replace $D_z|_{i,j,k+1/2}^{n+1/2}$ at $j=N$ as

$$D_z|_{i,N,k+1/2}^{n+1/2} \leftarrow D_z|_{i,0,k+1/2}^{n+1/2}. \tag{16}$$

Note that, in the y directional periodicity, no special PBC treatments are needed for other field components ($\mathbf{E}^{n+1/2}$, $\boldsymbol{\phi}^{n+1/2}$, $\mathbf{H}^{n+1/2}$, and $D_y^{n+1/2}$). Similar PBCs are straightforwardly applied for the x directional periodicity and the second-sub-step update equations. It is worthwhile to note that the cyclic tridiagonal matrix $[\mathbf{M}]$ in Eq. (12) can be applied for the case of $a \neq c$, differently from the previous literature (see Eq. (13) in [22]). To solve Eq. (12), the Sherman-Morrison algorithm [19, 23] is applied as what follows. Let us consider Eq. (12) as a perturbation of matrix $[\mathbf{N}]$ by the by following relation

$$[\mathbf{M}] = [\mathbf{N}] + \mathbf{w}\mathbf{z}^T, \tag{17}$$

$$[\mathbf{N}] = \begin{bmatrix} 2b_0 & c_0 & 0 & 0 & 0 \\ a_1 & b_1 & c_1 & 0 & 0 \\ 0 & \ddots & \ddots & \ddots & 0 \\ 0 & 0 & a_{N-2} & b_{N-2} & c_{N-2} \\ 0 & 0 & 0 & a_{N-1} & b_{N-1}+(c_1 a_{N-1}/b_0) \end{bmatrix},$$

$$\mathbf{w} = \begin{bmatrix} -b_0, & 0, & \cdots, & 0, & c_0, \end{bmatrix}^T, \quad \mathbf{z} = \begin{bmatrix} 1, & 0, & \cdots, & 0, & -a_{N-1}/b_0 \end{bmatrix}^T.$$

Then, we use the Thomas algorithm to evaluate two auxiliary vectors ($\mathbf{x}_1$ and $\mathbf{x}_2$)

$$[\mathbf{N}]\mathbf{x}_1 = \mathbf{r}, \tag{18}$$
$$[\mathbf{N}]\mathbf{x}_2 = \mathbf{w}. \tag{19}$$

After solving $\mathbf{x}_1$ and $\mathbf{x}_2$, the final update equation of D_x can be obtained via

$$\mathbf{x} = \mathbf{x}_1 + B\mathbf{x}_2, \tag{20}$$

where

$$B = -\frac{\mathbf{z}^T \mathbf{x}_1}{1 + \mathbf{z}^T \mathbf{x}_2}.$$
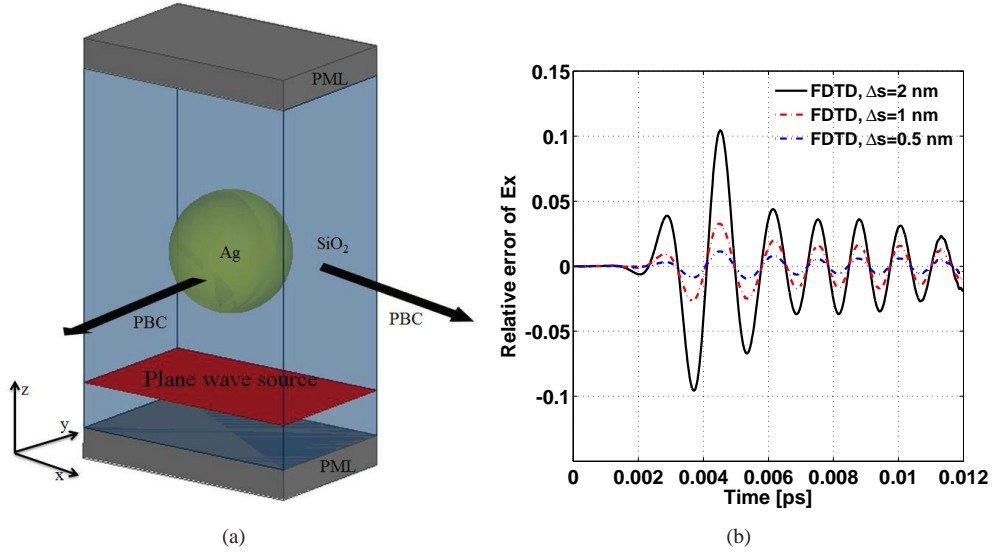
Fig. 2. (a) Geometry of the numerical example. (b) Convergence test of space-step sizes.

3. Numerical example

As a proof of concept of QCRF-ADI-FDTD, we analyze optical wave interaction with a square periodic array of Ag nanospheres (the Ag radius of 10 nm and the center-to-center distance of 40 nm) surrounded by SiO_2 under a normal incident x-polarized plane wave excitation (see Fig. 2(a)). The observation point is located at the center on a transverse plane and 5 nm below from the plane wave source plane. Ten CFS-PML layers are used for the z direction and the PBC is used for the x and y directions. The total physical domain is 40 nm $\times$ 40 nm $\times$ 60 nm. We set $A_0 = 112.62$, $A_1 = 7.224 \times 10^{-16}$, $A_2 = 1.364 \times 10^{-30}$, $B_1 = 3.108 \times 10^{-18}$ and $B_2 = 7.590 \times 10^{-31}$ for the QCRF coefficients of Ag. Note that we use a constant relative permittivity of 2.25 for SiO_2. We define the CFL number ($CFLN$) as $CFLN = \Delta t / \Delta t_{FDTD, \, max}$ and we use cubic cells ($\Delta s = \Delta x = \Delta y = \Delta z$). Before proceeding, we first perform a convergence test by varying the space-step sizes in FDTD simulations. The space-step sizes larger than 2 nm lead to high staircasing errors and the space-step sizes smaller than 0.25 nm lead to overwhelming computational costs. Therefore, we consider $\Delta s = 2$ nm, 1 nm, 0.5 nm, and 0.25 nm for the convergence test. Figure 2(b) shows the relative error of E_x field against the reference data (extracted from $\Delta s = 0.25$ nm) defined by $\left[E_x(t) - E_{x,ref}(t) \right] / |E_{x,ref}(t)|_{max}$ [1]. The maximum relative error is 10.44%, 3.28%, and 1.14% for $\Delta s = 2$ nm, 1 nm, and 0.5 nm respectively.

We first employ computational cells with $\Delta s = 0.5$ nm. Figure 3(a) shows the time response of E_x field and good agreement is observed between QCRF-FDTD and QCRF-ADI-FDTD up to $CFLN=8$. Figure 3(b) represents the relative error using QCRF-FDTD as reference, showing that the maximum relative error of QCRF-ADI-FDTD is 4.6%, 6.79%, and 14.09% for $CFLN=4$, 8, and 16 respectively. Next, we employ computational cells with $\Delta s = 0.25$ nm. Figure 4(a) shows the time response of E_x field and good agreement is observed between QCRF-FDTD and QCRF-ADI-FDTD up to $CFLN=16$. Figure 4(b) represents the relative error using QCRF-FDTD as reference, showing that the maximum relative error of QCRF-ADI-FDTD is 2.6%, 4.29%, and 7.45% for $CFLN=4$, 8, and 16 respectively. Figure 5 shows the snapshots of E_x field on the xy-plane at the center of the Ag nanosphere at the time instant of 0.0034795 ps, obtained from QCRF-FDTD with $CFLN=1$ and QCRF-ADI-FDTD with $CFLN=16$ for $\Delta s = 0.25$
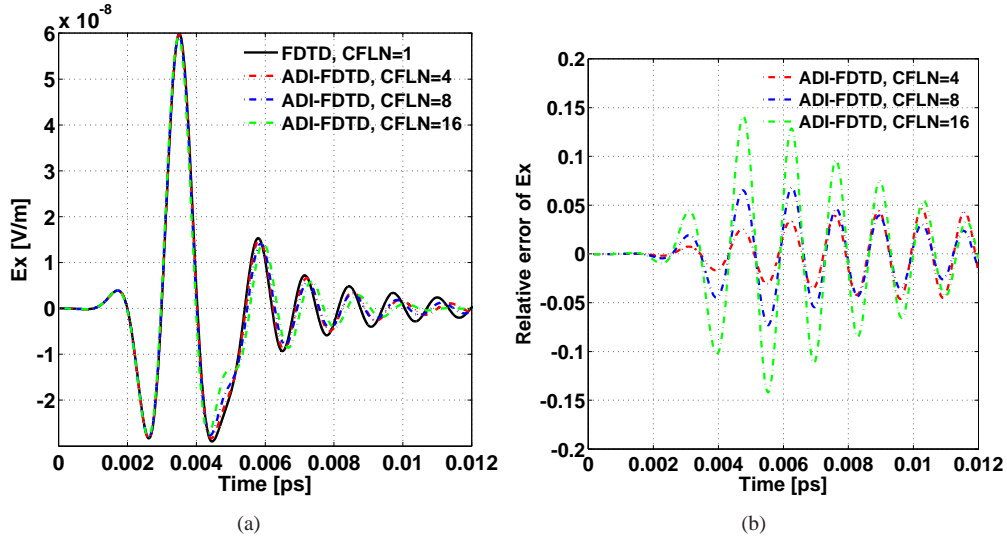
Fig. 3. (a) E_x field for Δs=0.5 nm. (b) Relative error of E_x field for Δs=0.5 nm.
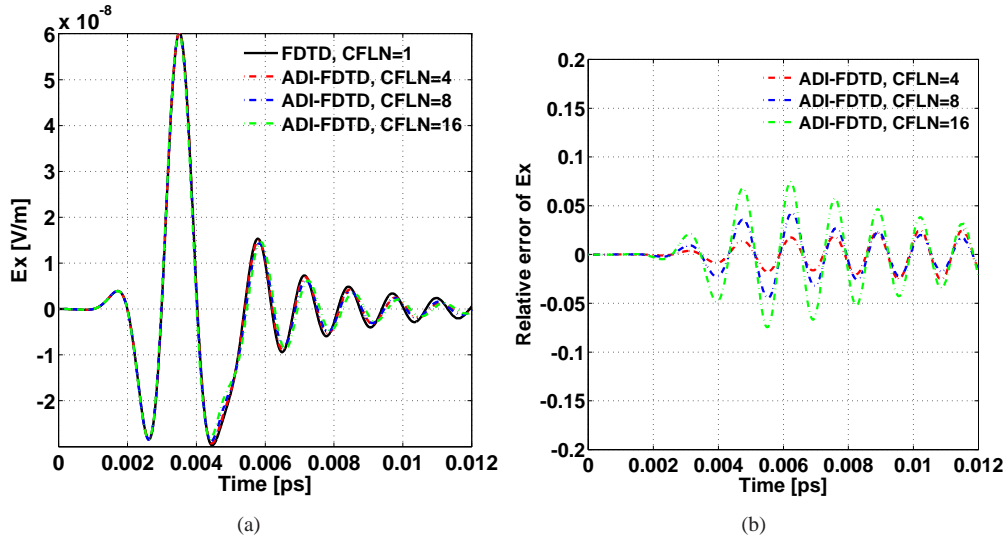

Fig. 4. (a) E_x field for Δs=0.25 nm. (b) Relative error of E_x field for Δs=0.25 nm.

nm. Overall, the field distribution of QCRF-ADI-FDTD agrees well with that of FDTD. We also calculate the L_2 relative error norm $\| \delta \|_2$ [24] of the field against the reference data (extracted from QCRF-FDTD) by

$$\| \delta \|_2 = \sqrt{\frac{\sum_{y=0}^{40nm} \sum_{x=0}^{40nm} \left(E_{x,ADI} - E_{x,FDTD}\right)^2}{\sum_{y=0}^{40nm} \sum_{x=0}^{40nm} \left(E_{x,FDTD}\right)^2}}. \tag{21}$$

It turns out that $\| \delta \|_2 = 6.92$ %. Finally, we compare the computational time of QCRF-ADI-FDTD normalized by the QCRF-FDTD counterpart in Fig. 6. Note that the CPU time of QCRF-ADI-FDTD with $CFLN$=8 is 56.17 % and that of QCRF-ADI-FDTD with $CFLN$=16 is 28.08
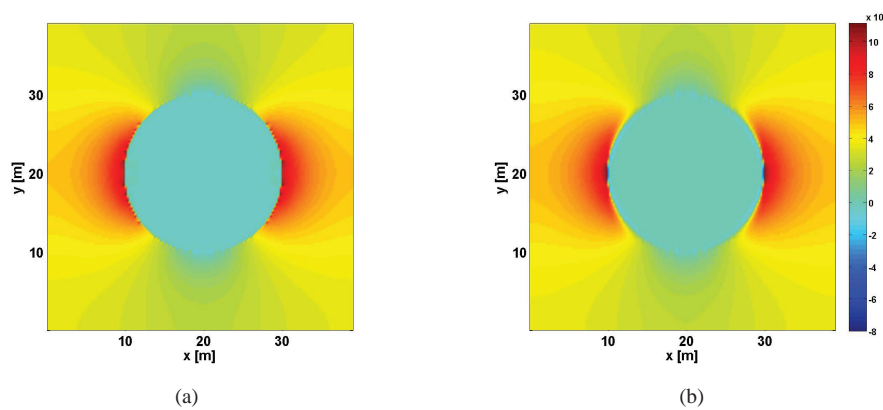
Fig. 5. Snapshot of E_x field for Δs=0.25 nm. (a) QCRF-FDTD with $CFLN$=1. (b) QCRF-ADI-FDTD with $CFLN$=16.
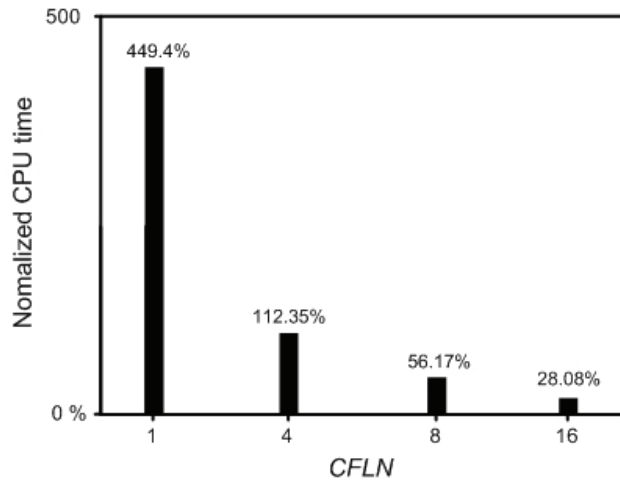

Fig. 6. Normalized CPU time of QCRF-ADI-FDTD.

%, compared to the QCRF-FDTD counterpart.

4. Conclusion

The QCRF dispersion model has been successfully applied to ADI-FDTD for the efficient optical analysis of dispersive media. In this work, the formulations of update equations and the PBC are derived in detail. The computational accuracy and efficiency of the proposed QCRF-ADI-FDTD is validated through the 3-D numerical example. For computational cells with Δs=0.25 nm, the QCRF-ADI-FDTD with $CFLN$=16 agrees well with the QCRF-FDTD counterpart, with the speedup enhancement of 3.56. QCRF-ADI-FDTD can be applied for the efficient optical analysis of electrically refined structures, such as nanowires, nanoholes, or plasmonic organic solar cells. It is also noting that the QCRF dispersion model can be extended to the pseudo-spectral time domain (PSTD) method [25–27].